

ELECTROMAGNETIC FIELDS GENERATED IN METALS BY THE QUASI STATIC PROPAGATION OF ELASTIC-PLASTIC CRACKS

P. N. B. ANONGBA

*U.F.R. Sciences des Structures de la Matière et de Technologie, Université
F.H.B. de Cocody, 22 BP 582 Abidjan 22, Côte d'Ivoire*

* Correspondance, e-mail : anongba@yahoo.fr

ABSTRACT

Starting from the well-established fact that the electric potential in metals round a dislocation is proportional to the associated lattice dilatation, we obtain by superposition the electric potential due to an isolated crack and a crack associated with a crack-tip plastic zone and a dislocation-free zone in between (elastic-plastic crack). We assume mode I loading in a linear isotropic elastic medium. The electric potential and associated electric field thus obtained, depend implicitly on time through the variation with time of the applied stress, crack length and size and location of the plastic zone. It is then possible, using Maxwell's equations, to obtain expressions for the induced magnetic field, Poynting's vector and intensity of the electromagnetic wave. We further restrict ourselves to quasi static propagation of the isolated crack assuming the Griffith condition $G = 2\gamma$ (G is the crack extension force and γ the surface energy) to hold at any time. Expressions and graphical representations of the various electromagnetic quantities are given; their explicit dependences with respect to various parameters including crack extension velocity and surface energy are revealed. The present study applies to pure metals. However, because an expression of the lattice dilatation is also obtained, this latter result can be used in any other material where an electric field is produced by an inhomogeneous dilatation of the lattice. The case of ice is discussed and it is indicated how an analysis, taking account of crack-tip plasticity, could be conducted. Finally, the weakness in certain models devoted to the emission of electromagnetic radiation during plasticity and fracture in metallic materials is stressed.

Keywords : *crack mechanics, crack propagation, dislocations, crack-tip plasticity, electromagnetic radiation*

P. N. B. ANONGBA

RÉSUMÉ

Champs électromagnétiques générés dans les métaux par la propagation quasi statique de fissures élastiques plastiques

Dans la présente étude, nous partons du résultat bien connu dans les métaux que le potentiel électrique généré par une dislocation est proportionnel à la dilatation du réseau qu'elle introduit, pour donner par superposition, le potentiel électrique produit par une fissure isolée et une fissure entourée d'une zone plastique localisée en tête de fissure entre lesquelles il y a une zone libre de dislocation (fissure élastique plastique). Nous considérons une sollicitation en mode I dans un milieu élastique linéaire isotrope. Le potentiel et champ électrique ainsi obtenus, dépendent implicitement du temps à travers la dépendance en fonction du temps de la contrainte appliquée, de la taille de la fissure et de la taille et localisation de la zone plastique. Il est alors possible, à partir des équations de Maxwell, d'en proposer une expression du champ magnétique induit et, par conséquent, du vecteur de Poynting et de l'intensité de l'onde électromagnétique associée. Nous nous restreignons ensuite à la propagation quasi statique d'une fissure isolée en supposant que la condition de Griffith $G = 2\gamma$ (G est la force d'extension de la fissure et γ l'énergie de surface) s'applique à tout instant. Des expressions de diverses grandeurs électromagnétiques et leur représentations graphiques sont données. Les dépendances explicites de ces grandeurs en fonction de divers paramètres, dont la contrainte appliquée, la vitesse de propagation du front de fissure et l'énergie de surface, sont mises en évidence. Les résultats de ce travail s'appliquent d'abord aux métaux. Comme ce travail fournit également une expression de la dilatation inhomogène du réseau, ce dernier résultat peut être également utilisé pour tout autre matériau où une dilatation du réseau produit un champ électrique. Le cas de la glace est discuté explicitement et il est indiqué comment une analyse prenant en compte une plasticité localisée en tête de fissure peut être menée. Finalement, la faiblesse de certains modèles, destinés à rendre compte de l'émission de rayonnements électromagnétiques dans les métaux, est démontrée.

Mots-clés: *mécanique de la rupture, propagation de fissure, dislocations, plasticité en tête de fissure, rayonnement électromagnétique.*

I - INTRODUCTION

Electromagnetic phenomena generated in materials by dislocations and cracks are known for more than half a century; a review of works on electrical effects of dislocations in various materials (ionic crystals, metals,

semiconductors) has been given by Nabarro [1] who also provides us with the following simple result valid for metals: the inhomogeneous dilatation $\Delta_D(\vec{x})$ (\vec{x} position vector) of the lattice due to the dislocation leads to a redistribution of the conduction electrons. As a result, an electric potential $V_D(\vec{x})$ and electric field $\vec{E}_D(\vec{x})$ are built round a dislocation; furthermore the relation linking Δ_D and V_D is linear.

The proportionality relation between V_D and Δ_D revealed in metallic materials is helpful. This suggests that a similar relation between the electric potential $V_C(\vec{x})$ (resp. V_{CD}) and the corresponding lattice dilatation $\Delta_C(\vec{x})$ (resp. Δ_{CD}) exists in presence of a crack (resp. elastic-plastic crack). This is because a crack is equivalent to a continuous distribution of dislocations with infinitesimal Burgers vectors (Bilby et al. [2]; Friedel [3]; Bilby and Eshelby [4]).

Our study aims at providing analytical expressions for V_C , V_{CD} and corresponding electric fields \vec{E}_C and \vec{E}_{CD} for simple crack geometries. We stress that these expressions depend implicitly on time through parameters such as applied stress, crack length and size of plastic zone ahead of the crack front. We can then link the electric fields to their induced magnetic fields through Maxwell equations and interpret in this way the corresponding electromagnetic phenomena. The results apply first to metals for which a number of works on the emission of electromagnetic radiation exist (Misra [5], Misra and Kumar [6], Jagasivamani and Iyer [7], among others). Our work also finds application in any material where proportionality exists between electric potential and lattice dilatation such as in ice (Petrenko [8, 9]; Evtushenko et al. [10]).

The present analysis demonstrates once again the conceptual advantage of representing the crack by a continuous distribution of infinitesimal dislocations. This allows a simplified treatment (calculation of electric polarization vector, electric potential and electric and magnetic fields, for instance) based on the dislocation only. Additional experiments of concern are numerous and involve a number of different materials (see for example: Golovin et al. [11]; Cress et al. [12]; Frid et al. [13]; Mori et al. [14]; Hadjicontis et al. [15]).

In what follows, an elastic-plastic crack model under mode I loading is considered (Section 2) from which an expression for the electric potential is calculated; the isolated crack is equally treated. In Section 3, the electric field, induced magnetic field and Poynting's vector are derived. In Section 4, graphical representations of the various electromagnetic quantities are performed for the isolated crack that propagates quasi statically. A discussion is made of our results in Section 5 followed by a conclusion (Section 6).

II - METHODOLOGY AND RESULTS

II-1. Model and electric potential

II-1-1. The model

The model we shall refer to is shown in **Figure 1**. This is a linear isotropic elastic medium to which we attach a Cartesian coordinate system x_i . It contains a planar crack in the Ox_1x_3 -plane that extends from $x_1 = -c$ to c and runs indefinitely in the x_3 -direction. Coplanar to the crack, and on both sides of it, a dislocation-free zone ($c < |x_1| < e$) and a localized crack-tip plastic zone ($e \leq |x_1| \leq a$) are present. This model originates from Bilby et al. [2] in their study of the spread of plastic yielding from a notch. They have introduced one common description of cracking and plasticity in terms of dislocations. Both the crack and the plastic regions are represented by continuous distributions of dislocations.

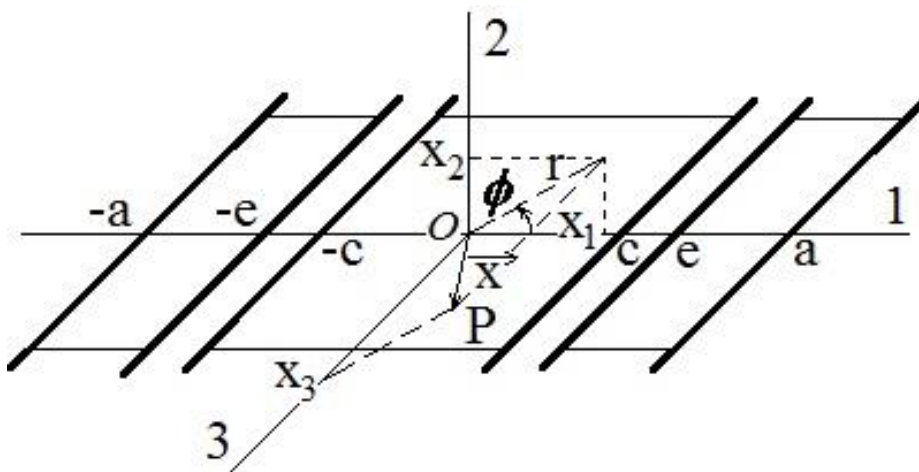


Figure 1: An elastic-plastic crack system located in the Ox_1x_3 -plane. The crack extends from $x_1 = -c$ to c with a straight front running indefinitely in the x_3 -direction. On both sides of the crack, a dislocation-free zone $c < |x_1| < e$ and plastic domain $e \leq |x_1| \leq a$ are present. The system is subjected to uniform applied tension σ_a in the x_2 -direction (see text).

Later on, a dislocation-free zone (DFZ) between the crack and the slip dislocations has been introduced into the analysis by Chang and Ohr [16- 18].

A DFZ allows high stresses to be attained at the tip of the crack, a necessary condition for brittle fracture propagation. This model of elastic-plastic crack explains quite well the relationship between applied stress, yield stress and parameters c , e and a (Bilby et al. [2]; Anongba and Vitek [19]). We can therefore expect this modelling to give appropriate values of the electromagnetic fields in presence of crack and localized plasticity at crack tip. In many experiments, dislocation generation is observed from the tip of the crack prior to crack motion. Anongba and Vitek [19] have shown that the condition $G = 2\gamma$ holds when the plastic zone is fixed at the initiation stage of crack propagation and they provide an appropriate expression for G .

We shall restrict ourselves to mode I loading only (uniform applied stress σ_a in the x_2 -direction). Both the crack and the plastic domain are mathematically represented by planar continuous arrays of infinitely long straight edge dislocations (Burgers vector $(0, b, 0)$, $b > 0$) lying parallel to the x_3 -axis. The dislocations are in equilibrium, can climb freely in the crack but must overcome a friction stress σ_y ($> \sigma_a$) representing the yield stress in the plastic region.

II-1-2. The electric potential

To calculate the electric potential, we assume as in metals (Section 1) that it is proportional to the dilatation of the lattice. We begin with the contribution due to a single dislocation and then, by superposition, display the results for the isolated crack (i.e. a crack with no plastic zone) and the elastic-plastic crack of **Figure 1**.

Consider an edge dislocation (Burgers vector $(0, b, 0)$) at the origin that lies indefinitely in the x_3 -direction. The dilatation Δ_D at a point P with coordinates (x_1, x_2, x_3) is proportional to $\sum_i \sigma_{ij}$ where (σ_{ij}) is the stress tensor.

In the present geometry, (σ_{ij}) may be taken from Anongba [20, 21] or Anongba et al. [22]; this gives

$$\Delta_D = \frac{b}{2\pi} \left(\frac{1-2\nu}{1-\nu} \right) \frac{\cos \phi}{r}; \quad (1)$$

ν is Poisson's ratio, r and ϕ are the associated cylindrical coordinates (see **Figure 1**) with $r^2 = x_1^2 + x_2^2$. In metallic materials, the electric potential $V_D(\vec{x})$, $\vec{x} = \overrightarrow{OP}$, round the dislocation is proportional to Δ_D as (Landauer [23]; Dexter [24]; Nabarro [1]; Brown [25]):

$$V_D(\vec{x}) = c_0 \frac{E_F}{q} \frac{b}{2\pi} \left(\frac{1-2\nu}{1-\nu} \right) \frac{\cos \phi}{r} \equiv A \frac{\cos \phi}{r}. \quad (2)$$

Here $E_F = \hbar^2 k_F^2 / 2m$ where k_F is the conduction electron wave number on the Fermi surface, m and q the electron mass and charge, \hbar has its usual meaning and c_0 is a constant, given by Nabarro [1] as $c_0 = 4/15$.

By superposition, the electric potential V_{CD} round the crack system in **Figure 1** can be written as

$$V_{CD}(\vec{x}) = A \left(\int_{-e}^{-a} + \int_{-c}^c + \int_e^a \right) \frac{x_1 - x_1'}{(x_1 - x_1')^2 - x_2^2} f_{CD}(x_1') dx_1' \quad (3)$$

where the dislocation distribution function $f_{CD}(x_1)$ is such that $f_{CD}(x_1)dx_1$ gives the number of dislocations in the interval dx_1 at the position x_1 ($|x_1| < c$ and $e < |x_1| < a$) and $f_{CD}(\pm e) = f_{CD}(\pm a) = 0$. Analytical expressions for f_{CD} have been given in different forms by Chang and Ohr [18] and Anongba and Vitek [19]; the latter expression appears simpler to deal with and will be adopted in the following. Before displaying the result of the integration in (3), we shall first write the electric potential V_C for the isolated crack (i.e. the crack of **Figure 1** only, without the plastic regions $e < |x_1| < a$).

Bilby and Eshelby [4] have given the distribution function of crack dislocations for the isolated crack to be $f_C(x_1) = \sigma_a x_1 / \pi C_1 \sqrt{c^2 - x_1^2}$ ($C_1 = \mu b / 2\pi(1-\nu)$, μ the shear modulus), that we use and, by integration, we obtain

$$V_C(\vec{x}) = (g_C(z) + g_C(\bar{z})) / 2 = \text{Re}[g_C(z)] \quad (4)$$

with

$$g_C(z) = \bar{A} \sigma_a \left(-1 + \frac{z^2}{\sqrt{z^2(z^2 - c^2)}} \right) \quad (5)$$

where $\bar{A} = A / C_1 = c_0(1-2\nu)E_F / \mu q$, $z = x_1 + ix_2$ is a complex variable and $\text{Re}[\dots]$ denotes the real part of the complex quantity inside the brackets [].

For the elastic-plastic crack of **Figure 1**, Anongba and Vitek [19] have given the dislocation distribution function f_{CD} in the form: for $|x_1| < c$,

$$f_{CD}(x_1) = \frac{2\sigma_y F(\pi/2, k)}{C_1 \pi^2} \left(\frac{(e^2 - c^2)x_1}{e\sqrt{a^2 - c^2}} \sqrt{\frac{a^2 - x_1^2}{(c^2 - x_1^2)(e^2 - x_1^2)}} + \operatorname{sgn}(x_1) Z(\beta_1(x_1), k) \right)$$

and

$$f_{CD}(x_1) = \frac{2\sigma_y F(\pi/2, k)}{C_1 \pi^2} \operatorname{sgn}(x_1) Z(\beta_2(x_1), k) \quad \text{for } e \leq |x_1| \leq a; \quad (6)$$

here

$$k^2 = c^2(a^2 - e^2)/e^2(a^2 - c^2), \quad \operatorname{sgn}(x_1) = x_1/|x_1|, \quad \beta_1(x_1) = \sin^{-1}(1/\sqrt{n(x_1)}), \\ \beta_2(x_1) = \sin^{-1}(\sqrt{n(x_1)}/k), \quad n(x_1) = c^2(e^2 - x_1^2)/e^2(c^2 - x_1^2)$$

and F and Z are the elliptic integral of first kind and Jacobi's zeta function, respectively. With the help of this expression for f_{CD} , we can perform the necessary integrations in (3) and write V_{CD} in the following form:

$$V_{CD}(\bar{x}) = (g_{CD}(z) + g_{CD}(\bar{z}))/2 = \operatorname{Re}[g_{CD}(z)] \quad (7)$$

with

$$g_{CD}(z) = 2(\bar{A}/\pi^2) \sigma_y F(\pi/2, k) \left(\frac{e^2 - c^2}{e^2(a^2 - c^2)} \left[-2a^2 \Pi(\pi/2, -\frac{c^2}{a^2 - c^2}, k) \right. \right. \\ \left. \left. + \frac{2(a^2 - e^2)F(\pi/2, k)z^2}{z^2 - e^2} + 2(c^2 - e^2) \frac{z^2(a^2 - z^2)}{(z^2 - e^2)(z^2 - c^2)} \Pi(\pi/2, n(z), k) \right] \right. \\ \left. + Z\ln(\pi/2, m(z), k) - Z\ln(\pi/2, n(z), k) + Z\ln(\pi/2, c^2/e^2, k) \right. \\ \left. - Z\ln(\pi/2, \frac{a^2 - e^2}{a^2 - c^2}, k) \right); \quad (8)$$

where

$$m(z) = (a^2 - e^2)(z^2 - c^2)/(a^2 - c^2)(z^2 - e^2), \quad n(z) = c^2(e^2 - z^2)/e^2(c^2 - z^2)$$

and Π and $Z\ln$ are the elliptic integral of third kind and a "special" function defined as (here ϕ , n and k are variables)

$$Z\ln(\phi, n, k) = \int_0^\phi \ln(1 - n \sin^2 \beta) dZ(\beta, k).$$

In this definition of $Z\ln$, \ln is the natural logarithm, dZ is the differentiation of the Jacobi's zeta function $Z(\beta, k)$ with respect to variable β only (i.e. $dZ \equiv (\partial Z / \partial \beta) d\beta$).

II-2. Electric and magnetic fields

The electric potential $V(\vec{x})$ and electric field $\vec{E}(\vec{x})$ are related by the relation $\vec{E} = -\overrightarrow{\text{grad}}V$; when, as in the present study, V can be written as $V(\vec{x}) = \text{Re}[g(z)]$ with $z = x_1 + ix_2$, we arrive at

$$\vec{E}(\vec{x}) = \begin{pmatrix} -\text{Re}[\partial g / \partial z] \\ \text{Im}[\partial g / \partial z] \\ 0 \end{pmatrix} \quad (9)$$

in the basis $(\vec{e}_1, \vec{e}_2, \vec{e}_3)$ of the Cartesian system $Ox_1x_2x_3$ (**Figure 1**). $\text{Im}[\dots]$ denotes the imaginary part of the function inside the brackets[]. \vec{E}_C and \vec{E}_{CD} are obtained from (9) with g taking the values g_C and g_{CD} respectively.

Because the electric field \vec{E} depends on parameters c , e , a and σ_a , it depends implicitly on time through the variation with time of these parameters. Consequently, an associated induced magnetic field \vec{B} exists that can be found from Maxwell's equations. In a linear isotropic medium, this induced \vec{B} is linked to \vec{E} by

$$\overrightarrow{\text{rot}} \left(\frac{\vec{B}}{\mu_0 \mu_1} \right) = \frac{\partial}{\partial t} (\varepsilon_0 \varepsilon_1 \vec{E}); \quad (10)$$

ε_0 and μ_0 are the electric and magnetic constants; ε_1 and μ_1 are the relative permittivity and permeability, respectively. Actually, we should add to the electric field an additional term \vec{E}' corresponding to the temporal variation of the magnetic field through the relation

$$\overrightarrow{\text{rot}} \vec{E}' = -\partial \vec{B} / \partial t. \quad (11)$$

Now assuming in a similar way as \vec{E} (9), \vec{E}' to be independent of x_3 with no component along the x_3 -direction, (11) leads to $\partial B_i / \partial t = 0$, $i = 1$ and 2 , where B_i is the component along the x_i -axis of \vec{B} . As a consequence B_i ($i = 1$ and 2) are constant with time and can be set equal to zero if initially there is no current. In the following, we shall restrict ourselves to the calculation of \vec{B} (10) assuming \vec{B} to be parallel to x_3 only. Also, \vec{E}' is viewed as of second order in magnitude, and will no more be considered. We thus obtain

$$\vec{B} = B_3 \vec{e}_3 = -\varepsilon_0 \varepsilon_1 \mu_0 \mu_1 (\partial \text{Im}[g(z)] / \partial t) \vec{e}_3. \quad (12)$$

Again, \vec{B}_C (isolated crack) and \vec{B}_{CD} (elastic-plastic crack, **Figure 1**) are obtained from (12) with g taking the values g_C and g_{CD} . We stress that we assume no current for simplicity. This applies to pure metals. Foreign ions, introduced into the lattice, could flow under the electric field and generate electric currents.

The Poynting's vector \vec{S} is the instantaneous energy that the electromagnetic wave transmits per unit time through a unit surface perpendicular to the direction of wave propagation. It reads

$$\begin{aligned} \vec{S} &= \vec{E} \wedge \frac{\vec{B}}{\mu_0 \mu_1} \\ &= \frac{B_3}{\mu_0 \mu_1} \begin{pmatrix} \text{Im}[\partial g / \partial z] \\ \text{Re}[\partial g / \partial z] \\ 0 \end{pmatrix} \end{aligned} \quad (13)$$

with \vec{S}_C , for the isolated crack, and \vec{S}_{CD} , for the elastic-plastic crack, both defined in a manner similar as previously.

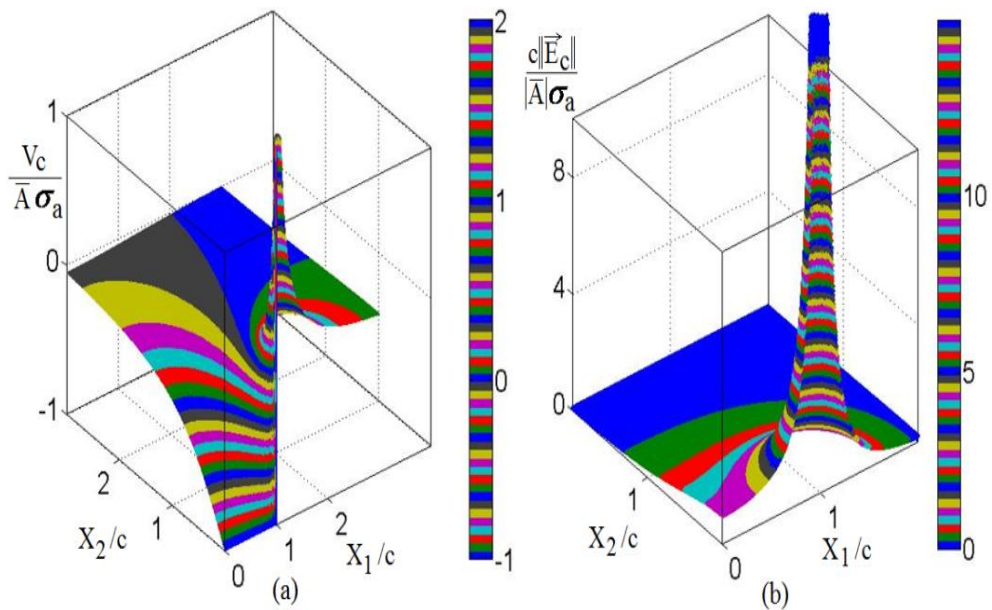
II-3. Quasi static propagation of an isolated crack

We consider here that the crack is isolated and we present graphical representations of various electromagnetic quantities. We restrict ourselves to the first quadrant (i.e. both x_1 and $x_2 \geq 0$) as justified into two steps: (1) g_C and $\partial g_C / \partial z$ are even and odd respectively, this reduces the domain to $-\pi/2 \leq \arg z \leq \pi/2$ (i.e. $x_1 \geq 0$). (2) Changing the sign of x_2 in g_C and $\partial g_C / \partial z$ is equivalent to taking their complex conjugates because z changes

into \bar{z} . Hence, in the expression of the electric field, $\text{Re}[\partial g_c / \partial z]$ remains unchanged while $\text{Im}[\partial g_c / \partial z]$ changes sign only. We can conveniently ascribe x_2 to positive values only.

II-3-1. Electric potential

The electric potential $V_C(\bar{x})$, shown in **Figure 2a**, is a surface that consists of various coloured bands. To each strip is associated a small range of values reported for convenience on a vertical scale (see in **Figure 2a**). In the Ox_1x_3 -plane ($x_2 = 0$), the electric potential is constant for $x_1 < c$ (zone occupied by the crack), blue colour at the bottom of the vertical scale to which is attached the value (-1). For $x_1 > c$, the potential, from zero (x_1 large), increases



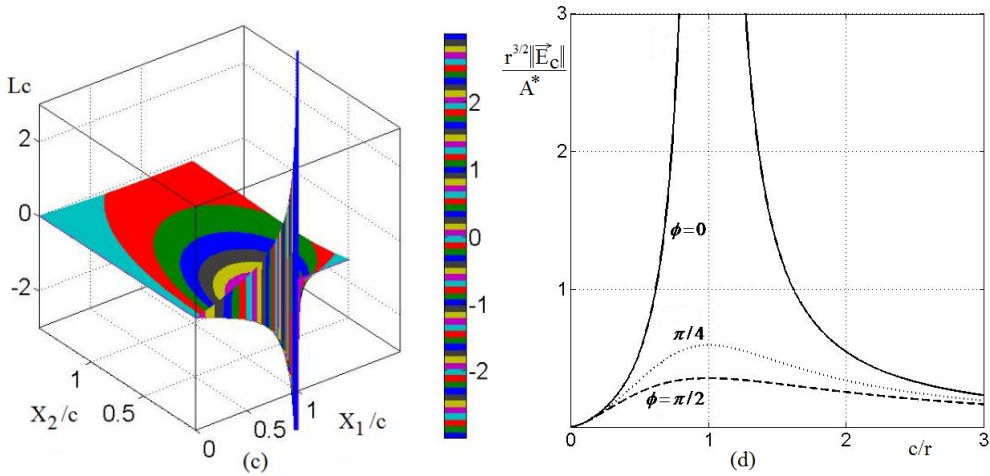


Figure 2: (a) Electric potential V_C (4). (b) Spatial distribution of the magnitude $\|\vec{E}_C\|$ of electric field (9)(14) at different (x_1, x_2) and (d) $\|\vec{E}_C\|$ values (17) calculated at three fixed positions $P(r, \phi, x_3)$, $\phi = 0, \pi/4$ and $\pi/2$, as a function of crack half-length c . We assume the Griffith relation(16) to hold at any time. (c) Lines of electric field $Lc = \text{constant}$ (15).

Indefinitely when x_1 tends towards the tip of the crack ($x_1 = c$). In the Ox_2x_3 -plane ($x_1 = 0$), the electric potential increases in the form of a parabola, from a value (-1) ($x_2 = 0$)(blue, at the bottom of the vertical scale), up to a value close to zero (brown) for x_2 large. In x_1x_2 planes ($x_3 = \text{constant}$), positive constant $V_C / \bar{A}\sigma_a$ contours have concentric shapes that shrink about the crack tip. The associated $V_C / \bar{A}\sigma_a$ values increase indefinitely.

II-3-2. Electric field

The electric field $\vec{E}_C(\vec{x})$ is given by (9) with

$$\frac{\partial g_C}{\partial z} = -\bar{A}\sigma_a \frac{c^2}{(z^2 - c^2)^{3/2}}. \quad (14)$$

At $P(r, \phi, x_3)$, the following points can be quoted:

- In the Ox_1x_3 -plane ($\phi = 0$), the x_1 -component of $\vec{E}_C, E_C(1)$, is equal to zero for $r < c$ because $\partial g_C / \partial z$ is pure imaginary. The reduced x_2 -component of $\vec{E}_C, E_C(2) / \bar{A}\sigma_a$, is then negative and given by

$$\frac{E_C(2)}{A\sigma_a} = -c^2 \sqrt{\frac{1}{(c^2 - r^2)^3}} .$$

For $r > c$, $\partial g_C / \partial z$ is pure real and $E_C(2)$ is zero while $E_C(1) / \bar{A}\sigma_a$ is positive and reads

$$\frac{E_C(1)}{A\sigma_a} = c^2 \sqrt{\frac{1}{(r^2 - c^2)^3}} .$$

- In the Ox_2x_3 -plane ($\phi = \pi/2$), $\partial g_C / \partial z$ is pure imaginary, $E_C(1)$ is identically zero and $E_C(2) / \bar{A}\sigma_a$ is negative and given by

$$\frac{E_C(2)}{A\sigma_a} = -c^2 \sqrt{\frac{1}{(c^2 + r^2)^3}} .$$

- For $0 < \phi < \pi/2$, the electric field \vec{E}_C is tangent to the lines of electric field at any point P , by definition; this corresponds to the condition $d\vec{x}(P) \wedge \vec{E}_C(P) = 0$ where $d\vec{x}(P)$ is an infinitesimal displacement vector. Using this condition, it is easy to show that the lines of field are given by

$$L_C(\vec{x}) = \text{Im}[g_C(z)] = \text{constant} . \quad (15)$$

Constant L_C contours are shown on **Figure 2c**. The sense of \vec{E}_C along these curves may be deduced from (9) and (14).

The spatial distribution of the magnitude $\|\vec{E}_C\|$ of the electric field is shown on **Figure 2b**. In Ox_1x_3 , $\|\vec{E}_C\|$ increases indefinitely when x_1 tends towards c from both sides. $\|\vec{E}_C\|$ takes a non-zero value (value 1.12, purple) for $x_1 = 0$; it decreases to zero for x_1 large (above c). In Ox_2x_3 , $\|\vec{E}_C\|$ decreases, from the value (1.12, purple) ($x_2 = 0$), towards zero when x_2 increases. In x_1x_2 ($x_3 = \text{constant}$), spatial positions corresponding to $\|\vec{E}_C\| = \text{constant}$, form circles that shrink about $x_1 = c$ with associated $\|\vec{E}_C\|$ increasing indefinitely.

We would like to express quantity $\|\vec{E}_C(P)\|$ at a given position $P(x_1, x_2, x_3)$ with cylindrical coordinates (r, ϕ, x_3) as a function of the crack half-length c . Because $\|\vec{E}_C\|$ depends on the applied stress σ_a , it is necessary to specify the dependence of σ_a with respect to c . In the present study, we shall assume that the Griffith relation $G = 2\gamma$ is satisfied at any time. This leads to

$$c = \frac{2\gamma E}{\pi(1-\nu^2)} \frac{1}{\sigma_a^2} \tag{16}$$

where E is Young's modulus. We can write, making use of (9), (14) and (16), that

$$\|\vec{E}_C(\vec{x})\| = A^* \left(\frac{c}{|z^2 - c^2|} \right)^{3/2} \tag{17}$$

with

$$A^* = \frac{c_0(1-2\nu)E_F}{\mu|q|} \sqrt{\frac{2\gamma E}{\pi(1-\nu^2)}}.$$

Figure 2d displays $\|\vec{E}_C\|$ for three different points $P(r, \phi, x_3)$, $\phi = 0, \pi/4$ and $\pi/2$, as a function of c . When $\phi = 0$, the point P lies in Ox_1x_3 , the plane of the crack. From the value $c = 0$, $\|\vec{E}_C\|$ increases (from the value zero) indefinitely when c tends towards P ($c \rightarrow r$). When $c > r$, $\|\vec{E}_C\|$ decreases gradually when c increases. For the two other positions of P , $\phi = \pi/4$ and $\pi/2$, $\|\vec{E}_C\|$ increases from zero ($c = 0$) up to a maximum for c about r ; then $\|\vec{E}_C\|$ decreases continually when c further increases in the range of large values.

II-3-3. Magnetic field

$B_3(\vec{x})$, the x_3 -component of the magnetic field (12), is represented in **Figure 3a** and **b**. We assume that g_c depends on time through σ_a and c ; we link σ_a to c by (16), this gives

$$B_3(\vec{x}) = \varepsilon_0 \varepsilon_1 \mu_0 \mu_1 A^* (dc/dt) c^{-3/2} \operatorname{Im} \left[-\frac{1}{2} \sqrt{\frac{z^2}{z^2 - c^2}} + c^2 \sqrt{\frac{z^2}{(z^2 - c^2)^3}} \right]. \quad (18)$$

In Ox_1x_3 ($x_2 = 0$), B_3 (**Figure 3a**) is zero for $x_1 > c$; for $x_1 < c$, B_3 has the shape of a parabola; it increases, from the value zero for $x_1 = 0$ (small strip of purple limited by the parabola), towards infinity when x_1 tends towards c . The corresponding stripes are displayed vertically and are limited by a parabola. Out of Ox_1x_3 ($0 < x_1 < c$), B_3 (**Figure 3a**) takes values close to zero (negative for both x_2 small and x_1 sufficiently close to c) and then increases slowly to reach a maximum when x_2 increases; further increase of x_2 leads to a decrease of B_3 . Out of Ox_1x_3 ($x_1 > c$), B_3 (**Figure 3a**) has negative values close to zero for x_2 small; when x_2 increases, B_3 first decreases up to a negative minimum (the magnitude of which increases as x_1 tends towards c); then B_3 increases from that minimum with x_2 . A boundary curve, that is

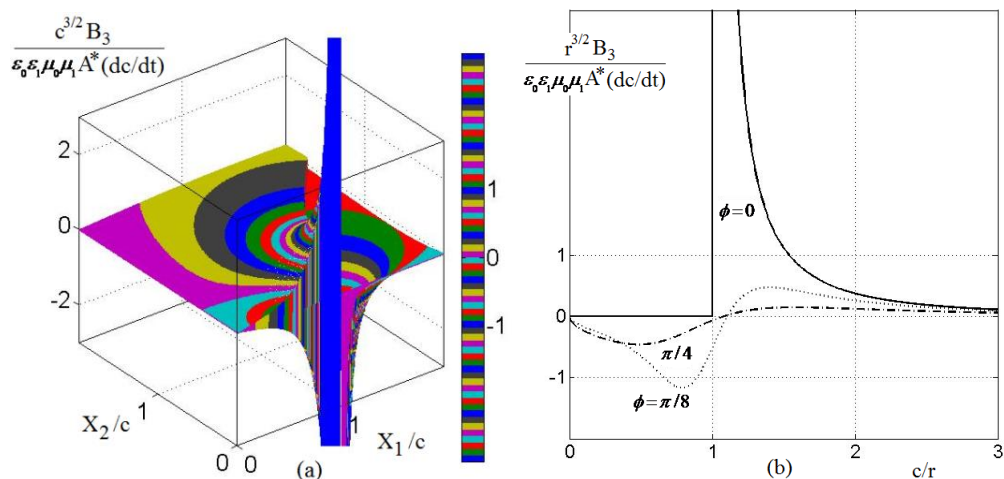


Figure 3: x_3 -component B_3 (18) of the magnetic field \vec{B}_c (12) for the isolated crack: (a) spatial distribution at different (x_1, x_2) for fixed crack half-length c and (b) B_3 values measured at three fixed positions $P(r, \phi, x_3)$, $\phi = 0, \pi/4$ and $\pi/8$, as a function of crack half-length c assuming the Griffith relation (16) to hold.

visible on Figure 3a, separates region 1 (with B_3 positive) from region 2 (with B_3 negative).

We have represented B_3 (**Figure 3b**) at three different positions $P(r, \phi, x_3)$ ($\phi = 0, \pi/4$ and $\pi/8$), as a function of crack half-length c . When $\phi = 0$ (i.e. P on the Ox_1x_3 plane) B_3 is zero for $c < r$. In the region $c > r$, B_3 increases indefinitely when c decreases towards r . For the two other positions of P , $\phi = \pi/4$ and $\pi/8$, B_3 (from the value zero for $c = 0$) displays a single oscillation with a negative minimum and positive maximum for $c < r$ and $c > r$ respectively. B_3 tends towards zero for large values of c . Note that for $\phi = \pi/2$ (Ox_2x_3 -plane, $x_1 = 0$), B_3 (18) is identically zero.

II-3-4. Poynting's vector

To illustrate the Poynting vector \vec{S} (13), we can make use of (18) for B_3 and (14) for $\partial g_c / \partial z$. In the Ox_1x_3 -plane ($x_2 = 0$), \vec{S} is equal to zero for $x_1 > c$ because B_3 is zero; for $x_1 < c$, $\partial g_c / \partial z$ (14) is pure imaginary, therefore the x_2 -component of \vec{S} is equal to zero because it is proportional to $\text{Re}[\partial g_c / \partial z] = 0$. Consequently, \vec{S} is parallel to the x_1 -direction and its sense is directed towards the tip of the crack. Observe that in the Ox_2x_3 -plane $\vec{S} = 0$ because B_3 is identically zero. Out of the Ox_1x_3 and Ox_2x_3 planes, it is convenient to make use of the lines of Poynting vector. We define a line of Poynting vector as a curve whose tangent at running point P is parallel to $\vec{S}(P)$. In a similar way as for the lines of electric field, we find that the lines of Poynting vector are given by the condition

$$Ls(\vec{x}) = \text{Re} \left[\sqrt{\frac{z^2}{z^2 - c^2}} \right] = \text{constant} . \tag{19}$$

Constant Ls contours are displayed on **Figure 4b**. The Poynting vector is tangent to these contours.

The intensity of the electromagnetic wave at position P is defined as the temporal average $\langle \|\vec{S}\| \rangle$ of the magnitude of the Poynting vector:

$$\langle \|\vec{S}\| \rangle = \frac{1}{T} \int_0^T \|\vec{S}\| dt \tag{20}$$

where T is a time interval for the integration. Assuming the crack to expand with time, with half lengths c_1 and c_2 at $t = 0$ and $t = T$ respectively, we can write (with the help of (12) and (13))

$$\langle \|\vec{S}\| \rangle = \varepsilon_0 \varepsilon_1 \langle v_c \rangle \frac{1}{c_2 - c_1} \int_{c_1}^{c_2} \left| \frac{\partial \text{Im}[g_c(z)]}{\partial c} \right| \left| \frac{\partial g_c(z)}{\partial z} \right| dc \quad (21)$$

where $\langle v_c \rangle = (c_2 - c_1)/T$ is the distance travelled by the crack divided by the travelling time T . $\langle v_c \rangle$ may be viewed as an average crack expansion velocity. With the help of (16) to (18), we can further manage $\langle \|\vec{S}\| \rangle$ to read

$$\langle \|\vec{S}\| \rangle = \frac{\varepsilon_0 \varepsilon_1 A^{*2} \langle v_c \rangle}{(c_2 - c_1)^3} \langle \tilde{s} \rangle \quad (22)$$

with

$$\langle \tilde{s} \rangle = \int_{\tilde{c}_1}^{\tilde{c}_1+1} \frac{1}{|\tilde{z}^2 - \tilde{c}^2|^{3/2}} \left| \text{Im} \left[-\frac{1}{2} \sqrt{\frac{\tilde{z}^2}{\tilde{z}^2 - \tilde{c}^2}} + \tilde{c}^2 \sqrt{\frac{\tilde{z}^2}{(\tilde{z}^2 - \tilde{c}^2)^3}} \right] \right| d\tilde{c} \quad (23)$$

where $\tilde{c}_1 = c_1/(c_2 - c_1)$ and $\tilde{z} = z/(c_2 - c_1)$.

The spatial distribution of $\langle \|\vec{S}\| \rangle$ is shown on **Figure 4a** ($c_1 = 0$ and $c_2 \equiv c$).

$\langle \|\vec{S}\| \rangle$ is relatively small outside the domain $[x_1 < c, x_2 < c]$ and increases considerably inside. Constant $\langle \|\vec{S}\| \rangle$ contours have an elliptical shape that shrinks gradually when $\langle \|\vec{S}\| \rangle$ increases. **Figure 4c** may provide a better understanding of the behaviour of $\langle \|\vec{S}\| \rangle$. On Figure 4c, we have reported $\langle \|\vec{S}\| \rangle$ (22), ($c_1 = 0$ and $c_2 \equiv c$) at three different points $P(r, \phi, x_3)$ ($\phi = \pi/8$, $\pi/4$ and $\pi/3$), as a function of the crack half-length c . The position with $\phi = \pi/8$ is closest to Ox_1x_3 , the plane occupied by the crack. The behaviour of

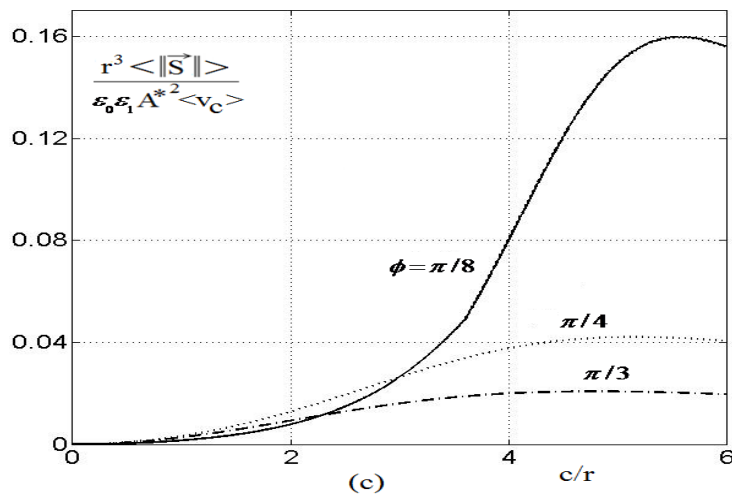
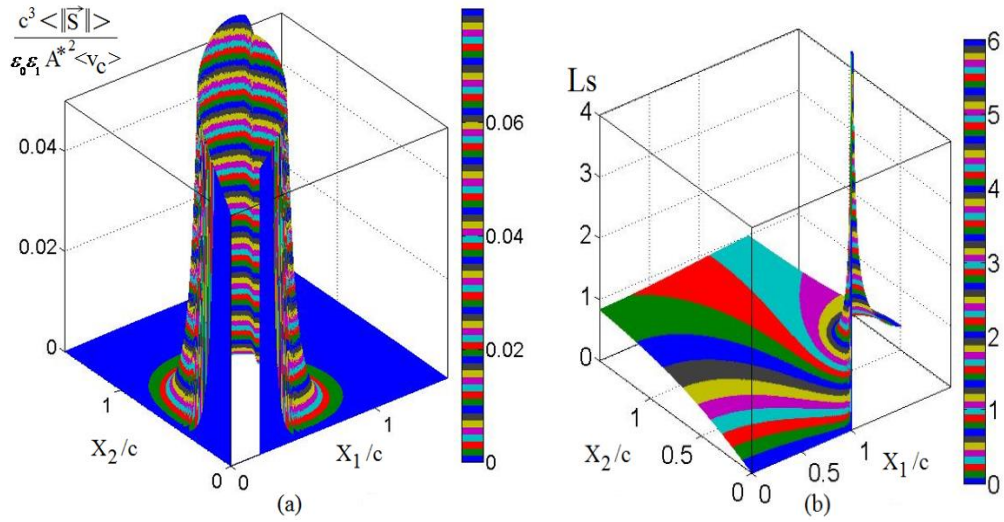


Figure 4: Intensity $\langle \|\vec{S}\rangle$ (22) of the electromagnetic wave: (a) spatial distribution at different (x_1, x_2) and (c) $\langle \|\vec{S}\rangle$ values measured at three fixed positions $P(r, \phi, x_3)$, $\phi = \pi/8, \pi/4$ and $\pi/3$, as a function of crack half-length c assuming the Griffith relation(16) to hold. (b) Lines of Poynting vector corresponding to $L_s = \text{constant}$ (19).

$\langle \|\vec{S}\rangle$ is common to all points. Starting from the value zero for $c=0$, $\langle \|\vec{S}\rangle$ increases with c up to a maximum at $c/r \cong 5.5$ for $\phi = \pi/8$ and then decreases slowly, the maximum of $\langle \|\vec{S}\rangle$ increasing rapidly when ϕ tends towards zero.

III - DISCUSSION

In absence of crack-tip plasticity (isolated crack), we have assumed the crack half-length c to depend implicitly on time and have linked σ_a to c through the Griffith relation $G = 2\gamma$. By doing so, we have introduced a quantity $dc/dt = v_c$, the velocity of the tip of the crack. The equilibrium condition requires that v_c be constant (quasi static crack propagation). A similar procedure can be adopted when the crack is elastic-plastic (**Figure 1**) but we have different possible scenarios (A and B, for example) with respect to the variation with time of the various parameters c , e , a and σ_a :

- A. We may assume that c is constant and a varies with time; then σ_a is linked to a through Chang and Ohr [18] condition that imposes a finite stress at the plastic zone boundaries (see also Anongba and Vitek [19] for the form below):

$$\frac{\pi\sigma_a}{2\sigma_y} = \frac{e^2 - c^2}{e\sqrt{a^2 - c^2}} \Pi(\pi/2, e^2k^2/c^2, k) \quad (24)$$

(for the definition of the various parameters, see (6)). The experimental situation corresponds to a spreading of the plastic zone under loading while the crack length is fixed. This treatment introduces a new parameter $da/dt = v_a$.

- B. This scenario corresponds to c variable, while the plastic zone is fixed at the initiation stage of fracture propagation. We can then proceed by making use of the Griffith relation $G = 2\gamma$ with the appropriate value of the crack extension force G given by Anongba and Vitek [19].

The resulting temporal dependences (so far described) for the electromagnetic fields correspond to quasi static changes of the configuration of the crack systems.

With regard to the application of the results of the present study, it is appropriate to refer first to ice. Because Evtushenko et al. [10] and Petrenko [8, 9] attribute some importance to lattice dilatation as a possible cause for the emission of electromagnetic radiation observed during the fracture of ice under loading. They propose expressions for the electric potential and electric field that involve lattice dilatation. The dilatation Δ_{CD} is related to V_{CD} (7) by

$$\Delta_{CD}(\vec{x}) = (q/c_0 E_F) V_{CD}(\vec{x}). \quad (25)$$

Introducing Δ_{CD} (25) into previous results for ice (see for example Petrenko [8, 9]) allows a treatment of the emission of electromagnetic radiation in ice when both cracks and plastic zones are present. Note that the yield stress σ_y is taken into account by the modelling. In absence of plasticity, the dilatation Δ_C and the electric potential V_C are also related by (25). Petrenko [9] has performed the following experiment in ice: fracture specimens with edge notch are subjected to tensile tests in which the applied stress is oscillatory; the associated electric potential is measured at different positions round the notch. Agreement between measured and calculated values of the potential is obtained. The electric potential is proportional to the dilatation of the lattice.

Petrenko [8, 9] did not discuss quasi static crack propagation on the line expounded in Section 4 that uses the Griffith $G = 2\gamma$ criterion to link the crack length to the applied stress. The treatment in Section 4 is of interest because physical quantities are revealed: crack-front velocity dc/dt , average crack extension velocity $\langle v_c \rangle$ and surface energy γ . The parameter A^* is proportional to $\sqrt{\gamma}$. Hence $\|\vec{E}_C\|$ (17) and $\|\vec{B}_C\|$ (i.e. $|B_3|$ (18)) are proportional to $\sqrt{\gamma}$ (**Figure 2d** and **3a** and **b**, respectively); the corresponding intensity $\langle \|\vec{S}\| \rangle$ (22) of the electromagnetic wave is proportional to γ (**Figure 4a** and **c**). $\|\vec{B}_C\|$ is proportional to dc/dt (**Figure 3a** and **b**) and $\langle \|\vec{S}\| \rangle$ (22) to $\langle v_c \rangle$ (**Figure 4a** and **c**). As the crack is expanding with time (i.e. c), electromagnetic quantities increases in magnitude up to a maximum and then decreases slowly at large distances far away from position P (see **Figure 2d** for $\|\vec{E}_C\|$ and **Figure 4c** for $\langle \|\vec{S}\| \rangle$). The component $|B_3|$ of the magnetic field on the over hand displays a single oscillation (**Figure 3b**). Petrenko [9] reports two types of signals (recorded by antenna) captured from a growing crack. Type 1 signal increases during crack propagation up to a maximum and then relaxes after crack arrest. Type 2 signal displays oscillations. Both types

of signal have been attributed to pre-existing intrinsic electric fields in ice although type 1 signal could correspond to quasi static propagation of the crack. This suggests re-examination of measured signals.

With regard to the dependence of the electromagnetic fields upon surface energy, we may refer to the experimental work of Misra and Kumar [6] with metallic materials. These authors have measured a linear variation of the electromagnetic radiation peak voltage with bond energy; this agrees with the proportionality between $\langle \|\vec{S}\| \rangle$ (22) and γ given by the present analysis (Section 4). Similarly, attention should be paid to experimental evidence of the dependence of the electromagnetic fields upon crack extension velocity. This brings us, for example, to the work by Frid et al. [13]: these authors have found an empirical equation that fits quite well electromagnetic radiation signals displaying oscillations in the form of a pulse. The signals are recorded during compression fracture of rocks (carbonate and igneous) and transparent materials (glass, PMMA and glass ceramics). They propose a derivation of the envelope of the pulse that is found to be proportional to the average crack velocity. In their modelling, they assume the envelope of the pulse to be associated with the fracture process itself and signal oscillations to vibration of charge carriers about equilibrium positions. This agrees with the result that the intensity of the electromagnetic wave $\langle \|\vec{S}\| \rangle$ (22) is proportional to the average crack velocity $\langle v_c \rangle$.

Actually the results of the present study find application as long as the dilatation of the lattice caused by dislocations and cracks produces an electric potential. This is believed to be the case in metals (Nabarro [1]; Molotskii [26]; Misra et al. [27]) in addition to ice (Evtushenko et al. [10]; Petrenko [8, 9]). The emission of electromagnetic radiation in metals has been observed in a number of different situations: at the onset of plastic flow, at different deformation stages on the stress-strain curves, at the initiation stage of crack propagation (for a review, see Misra et al. [27]). For these various situations, one must first find an appropriate model of the arrangement and dynamics of the dislocations and then proceed to calculate the associated lattice dilatation; in general, this is a formidable task. The model in *Figure 1* is presumably suitable in the situation of localized plasticity at the tip of the crack. Detailed confrontation with experiment is missing at present. Because available experimental works do not connect the emission of electromagnetic radiation with the size and location of crack-tip plastic zones.

Recently, Misra et al. [27] have proposed a theoretical model for the emission of electromagnetic radiation associated with plasticity and fracture in metallic materials. This work is based on a proposal made earlier by Molotskii [26]

that imposes the dislocation dipole moment to be proportional to the whole length of the dislocation. We first stress the weakness of this assumption and then indicate some difficulties with the modelling by Misra et al. [27].

Molotskii [26] working hypothesis can be described as follows. Assume a straight edge dislocation at the origin lying along the x_3 -direction (use *Figure 1* for the x_i -directions) with Burgers vector $(b,0,0)$ in the x_1 -direction. Under action of an applied stress, at a given time, its shape in the glide plane Ox_1x_3 is given at position $(0,0,x_3)$ by $\xi(x_3,t)$. He then considers that the dislocation, at any time, has a dipole moment p per unit length constant, independent of position x_3 . By doing so, Molotskii [26] finds that the dipole moment of the dislocation is proportional to the dislocation length and increases for small deviation from the straight edge position. Molotskii's result is difficult to accept because the dipole moment per unit length of a dislocation is associated with the dilatation of the lattice (Nabarro [1]) and therefore depends on dislocation character; it decreases to zero for screws in linear elasticity (the lattice dilatation for screws is zero).

To see the weakness of Molotskii's assumption that the dislocation dipole moment increases with its length, consider a straight edge dislocation segment with length $L = AB$ along Ox_3 that bows out in its glide plane from its initial straight edge position. The result is an increase of the dislocation length. Now assume its curved shape to consist of edge and screw portions only. Because all the screw portions have zero dipole moment, we discover that the curved dislocation has a dipole moment essentially identical to that of the segment AB along Ox_3 , contrary to Molotskii's working assumption.

Misra et al. [27] investigate electromagnetic radiation as a function of deformation up to fracture propagation using specimens with edge notch tested in tension. Plastic yielding from the notch precedes crack propagation. A specimen geometry with edges (see *Figure 1* to *3* in Misra et al. [27]) is used to elaborate a theoretical analysis that presents serious difficulties (*A* and *B*):

- A. According to Misra et al. [27] the straight edge dislocation is parallel to Oz , has Burgers vector along Ox and is associated with a supplementary half-plane of atoms Oyz ($y > 0$). The dipole moment of the dislocation is parallel to Oy . As the dislocation bows out with time from the straight edge position in the Oxz slip plane, its whole curved shape can be approximated by small straight edge and screw portions. The edge portions all have a dipole moment parallel to Oy and the screws contribute nothing. Consequently the variation with time of the

dipole moment of the dislocation remains parallel to Oy . It is impossible for the considered gliding edge dislocation to have the first temporal derivative of the dipole moment in the z -direction as assumed without any demonstration by the authors. We stress that a variation of the dislocation dipole moment lying in the z -direction would imply necessarily a spreading of the dislocation in the Oyz plane which contains both the dipole moment and the dislocation line direction Oz ; this corresponds to a climbing motion of the edge dislocation, a mechanism that is not considered by the authors.

- B. Misra et al. [27] also use the incorrect assumption of Molotskii [26] that stipulates that the dislocation dipole moment increases with its length.

In view of the difficulties indicated above, treatments by Molotskii [26] and Misra et al. [27] appear to be incorrect.

IV - CONCLUSION

This work provides formulas for the lattice dilatation, electric potential and electric field corresponding to an elastic-plastic crack and a brittle crack without crack-tip plasticity, under mode I loading. Taking account of an implicit variation with time of these quantities, this work gives expressions for the induced magnetic field and the associated Poynting vector. The results are applied to the quasi static propagation of an isolated crack assuming the Griffith condition $G = 2\gamma$ to hold; this reveals the relationships between the electromagnetic fields and various parameters such as crack-tip velocity and surface energy. It is indicated how a similar application can be performed when the crack is associated with a plastic zone; this would provide a better interpretation of experimental findings. The present study applies first to pure metals but could be adapted to any material where lattice dilatation produces an electric field: ice is discussed as one example. Finally the inadequacy of a number of models, proposed to explain the emission of electromagnetic radiation in metallic materials, is demonstrated.

RÉFÉRENCES

- [1] - F.R.N. NABARRO, "Theory of crystal dislocations", Oxford University Press, Oxford (1967)
- [2] - B.A. BILBY, A.H. COTTRELL and K.H. SWINDEN, *Proc. R. Soc. A.*, 272 (1963) 304-314
- [3] - J. FRIEDEL, "Dislocations", Pergamon Press, Oxford (1964)
- [4] - B.A. BILBY and J.D. ESHELBY, In: "Fracture", Ed. *Academic Press (H. Liebowitz)*, New York, Vol 1 (1968) 99 - 182
- [5] - A. MISRA, *Nature (London)*, 254 (1975) 133-134
- [6] - A. MISRA and A. KUMAR, *Int. J. Fract.*, 127 (2004) 387-401
- [7] - V. JAGASIVAMANI and K.J. IYER, *Mater Lett.*, 6 (1988) 418-421
- [8] - V.F. PETRENKO, *Philos. Mag. B*, 67 (1993) 301-315
- [9] - V.F. PETRENKO, *Special Report 96-2, US Army Corps of Engineers (CRREL)*, (1996) 1-30
- [10] - A.A. EVTUSHENKO, N. MAENO, V.F. PETRENKO and I.A. RYZHKIN, *J. de Physique C 1*, 48(3) (1987) 109-113
- [11] - Y.I. GOLOVIN, T.P. D'YACHEK, V.I. ORLOV and Y.I. TYALIN, *Fiz. Tverd. Tela (Leningrad)*, 27 (1985) 1110-1115
- [12] - G.O. CRESS, B.T. BRADY and G.A. ROWELL, *Geophys. Res. Lett.*, 14 (1987) 331-334
- [13] - V. FRID, A. RABINOVITCH and D. BAHAT, *J. Phys. D Appl. Phys.*, 36(13) (2003) 1620-1628
- [14] - Y. MORI, Y. OBATA, J. PAVELKA, J. SIKULA and T. LOKAJICEK, *J. Acoustic Emission*, 22 (2004) 91-101
- [15] - V. HADJICONTIS, C. MAVROMATOU and D. NINOS, *Nat. Hazards Earth Syst. Sci.*, 4(5) (2004) 633-639
- [16] - S.-J. CHANG and S.M. OHR, *J. Appl. Phys.*, 52 (1981) 7174-7181
- [17] - S.-J. CHANG and S.M. OHR, *J. Appl. Phys.*, 53 (1982) 5645-5651
- [18] - S.-J. CHANG and S.M. OHR, *Int. J. Fract.*, 23 (1983) R3-R6.
- [19] - P.N.B. ANONGBA and V. VITEK, *Int. J. Fract.*, 124 (2003) 1 - 15
- [20] - P.N.B. ANONGBA, *Rev. Ivoir. Sci. Technol.*, 14 (2009) 55 - 86
- [21] - P.N.B. ANONGBA, *Rev. Ivoir. Sci. Technol.*, 16 (2010) 11 - 50
- [22] - P.N.B. ANONGBA, J. BONNEVILLE and A. JOULAIN, *Rev. Ivoir. Sci. Technol.*, 17 (2011) 37 - 53
- [23] - R. LANDAUER, *Phys. Rev.*, 82 (1951) 520-521
- [24] - D.L. DEXTER, *Phys. Rev.*, 85 (1952) 936-937
- [25] - R.A. BROWN, *Phys. Rev.*, 141 (1966) 568-572
- [26] - M.I. MOLOTSKII, *Soviet Tech. Phys. Lett.*, 6 (1980) 22-23
- [27] - A. MISRA, R.C. PRASAD, V.S. CHAUHAN and B. SRILAKSHMI, *Int. J. Fract.*, 145 (2007) 99-121